BIOCHEMISTRY
including biophysical chemistry & molecular biology

Article

pubs.acs.org/biochemistry

The Myosin Duty Ratio Tunes the Calcium Sensitivity and Cooperative Activation of the Thin Filament

Milad Webb,[†] Del R. Jackson, Jr.,[†] Travis J. Stewart,[‡] Samuel P. Dugan,[‡] Michael S. Carter,[‡] Christine R. Cremo,[‡] and Josh E. Baker*[,†,‡]

[†]Department of Electrical and Biomedical Engineering, University of Nevada, Reno, Reno, Nevada 89557, United States

[‡]Department of Biochemistry and Molecular Biology, University of Nevada School of Medicine, Reno, Nevada 89557, United States

Supporting Information

ABSTRACT: In striated muscle, calcium binding to the thin filament (TF) regulatory complex activates actin−myosin ATPase activity, and actin−myosin kinetics in turn regulates TF activation. However, a quantitative description of the effects of actin−myosin kinetics on the calcium sensitivity (pCa_{50}) and cooperativity (n_H) of TF activation is lacking. With the assumption that TF structural transitions and TF−myosin binding transitions are inextricably coupled, we advanced the principles established by Kad et al. [Kad, N., et al. (2005) *Proc. Natl. Acad. Sci. U.S.A. 102*, 16990−16995] and Sich et al. [Sich, N. M., et al. (2011) *J. Biol. Chem. 285*, 39150−39159] to develop a simple model of TF regulation, which predicts that pCa_{50} varies linearly with duty ratio and that n_H is maximal near physiological duty ratios. Using *in vitro* motility to determine the calcium sensitivity of TF sliding velocities, we measured pCa_{50} and n_H at different myosin densities and in the presence of ATPase inhibitors. The observed effects of myosin density and actin−myosin duty ratio on pCa_{50} and n_H are consistent with our model predictions. In striated muscle, pCa_{50} must match cytosolic calcium concentrations and a maximal n_H optimizes calcium responsiveness. Our results indicate that pCa_{50} and n_H can be predictably tuned through TF−myosin ATPase kinetics and that drugs and disease states that alter ATPase kinetics can, through their effects on calcium sensitivity, alter the efficiency of muscle contraction.

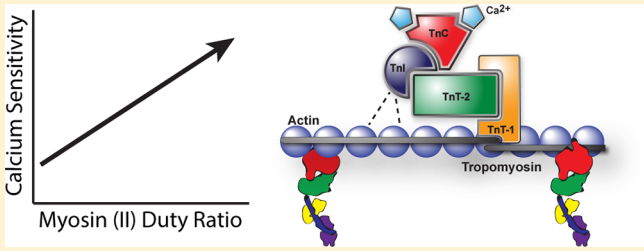

Calcium activation of striated thin filaments (TFs) is a highly regulated process critical for proper muscle function; however, knowledge of how myosin ATPase kinetics affects this regulatory process is relatively limited. TFs are activated by both calcium binding to the regulatory protein complex and myosin binding to actin.[1−3] When calcium binds to troponin-C (TnC), the C-terminal region of troponin-I moves from a binding site on actin to the open E-F hands of TnC, allowing the tropomyosin−troponin regulatory complex to move away from myosin binding sites on the TF.[4−9] The partially blocked, calcium-induced state becomes fully active when myosin binding further displaces the regulatory complex from myosin binding sites on actin.[10,11]

Nearly 40 years ago, it was shown that TFs are activated by rigor myosin crossbridges.[12] This phenomenon was again demonstrated using NEM-modified myosin S1.[13,14] More recently it has been shown that changes in actin−myosin attachment kinetics and changes in the number of myosin heads available to bind a TF also influence TF activation.[15−17] These studies all suggest that rate constants for intermediate steps in the TF−myosin ATPase cycle influence the regulation of striated muscle mechanics, yet a concise relationship among calcium sensitivity (pCa_{50}, pCa at half-maximal velocity), cooperativity (n_H, Hill coefficient), and ATPase kinetics has yet to be defined.

Conventional models describe TF activation though a series of TF structural transitions that are temporally separated from actin−myosin biochemical transitions.[10,18] For example, the three-state model of McKillop and Geeves[10] (Figure 1, solid arrows) describes biochemical transitions (left to right) that occur only within a given TF structural state (top to bottom). This formal separation of TF structural transitions from TF−myosin kinetic transitions allows one to incorporate structural data into kinetic models. However, in the absence of accurate descriptions of the interplay between TF and myosin structural dynamics, these models remain unconstrained by poorly defined structural parameters. Attempting to improve these models by adding more structural states or by introducing dynamics to one protein in the system increases the number of unconstrained parameters in the model.

Chemical kinetics implicitly deals with protein structural dynamics; by defining only chemical (not structural) states, our simple model of TF regulation (Figure 1, dashed arrow) avoids the challenge of formally untangling chemistry and structure. According to this model, TF activation occurs with a single kinetic step that implicitly accounts for all TF (and myosin)

Received: March 1, 2013
Revised: August 9, 2013
Published: August 15, 2013

dx.doi.org/10.1021/bi400262h | *Biochemistry* 2013, 52, 6437−6444

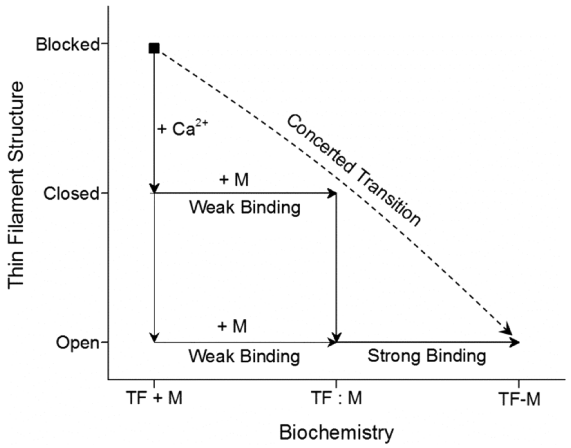

Figure 1. Sequential vs simple models of TF activation. According to sequential models, TF structural transitions (vertical arrows) are formally separated from TF−myosin biochemical transitions (horizontal arrows). Here three structural states (blocked, closed, and open) and three biochemical states (detached, weakly bound, and strongly bound) are illustrated. In a simple model (developed here), TF−myosin binding is modeled as a single kinetic transition (···) that implicitly deals with all TF structural changes associated with TF−myosin binding. Although here we assume only two chemical states, the weak-binding intermediate can be incorporated into a simple model by defining the rate of weak binding as a function of calcium and the number of weakly bound myosin heads.

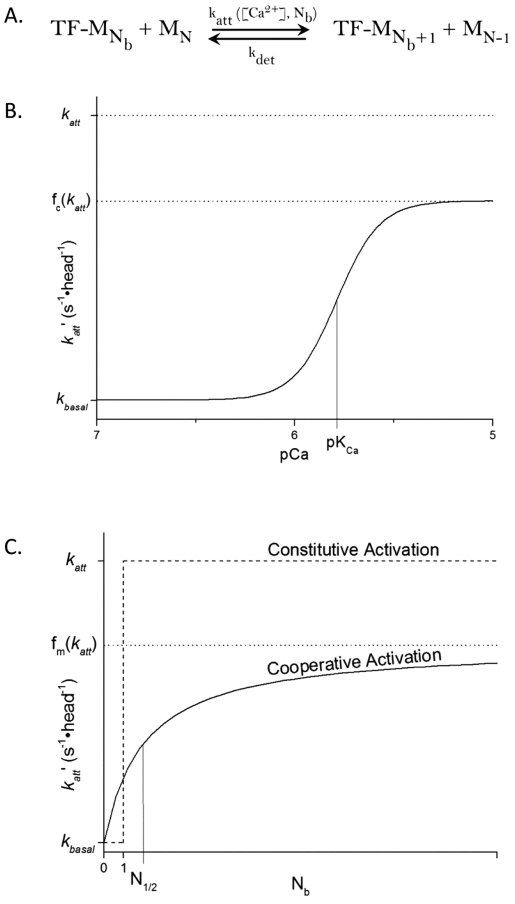

Figure 2. Combined effects of calcium- and myosin-dependent activation. (A) We propose a simple two-state binding reaction in which the rate of TF−myosin dissociation, k_{det}, dictates TF sliding velocity and k_{att} is a function of both Ca^{2+} and the number of myosin heads bound (N_b) to a TF. M_N represents the pool of free myosin, and M_{N_b} represents myosin strongly bound to a TF. (B) We assume that the rate of TF−myosin binding, k_{att}, has a Ca^{2+} dependence that follows the Hill equation (—). We assume a basal rate, k_{basal}, of activation in the absence of calcium and TF-bound myosin. We assume that the maximal calcium-induced activation is a fraction, f_c, of the maximal rate constant, k_{att}, for TF−myosin binding. K_{Ca} is the calcium dissociation constant for the TnC−Ca^{2+} species in the absence of myosin. (C) Previously,[17] we assumed that k_{att} (---) was constitutively activated by myosin binding (complete TF activation when $N_b > 0$). Here we assume that k_{att}' increases smoothly with N_b (—), reaching a half-maximum at $N_b = N_{1/2}$ and a maximum of $f_m k_{att}$ in the absence of calcium (···). When both f_m and f_c are <1, both calcium and myosin are needed for maximal activation.

structural changes associated with crossbridge formation (Figure 1, dashed arrow). Here we treat the weak-binding state (Figure 1, A:M) as an intermediate in a single TF−myosin strong binding step. The effective rate constant, k_{att}, for this step (Figure 2A) is influenced independently by calcium (Figure 2B) and myosin strong binding (Figure 2C).

The simple model was first described by Kad et al.,[15] and the effects of calcium were subsequently incorporated.[17] In both studies, we assumed that strong binding of a single myosin head fully activates the thin filament (Figure 2C, constitutive). Because myosin is known to cooperatively activate the TF,[19] the purpose of this investigation is to extend the method of Kad et al., and subsequently Sich et al., by incorporating myosin-based cooperative activation. A second goal is to use computer simulations based on this model to establish relationships among pCa_{50}, n_H, and TF−myosin ATPase kinetics.

Our simulations show that n_H varies with myosin duty ratio, r, yielding a maximal value near physiological duty ratios.[20] This change in n_H need not result from a change in calcium−TnC affinity, as is often assumed,[12,21−25] but can be caused by myosin-based activation (Figure 2C) alone.

We have previously shown that myosin ATPase kinetics mediates pCa_{50},[17] but we failed to establish an expression for pCa_{50} as a function of ATPase kinetics. The observation that ATPase kinetics influences pCa_{50} implies that the contractile component in muscle models cannot be treated as a black box that passively responds to calcium. A clear expression relating pCa_{50} and ATPase kinetics is needed. Here, our simulations show a simple relationship between ATPase kinetics and pCa_{50}. Specifically, pCa_{50} varies linearly with the product of the actin−myosin duty ratio, r, and the number, N, of myosin heads available to bind the thin filament.

We use *in vitro* motility (IVM) to test these relationships. We measured the calcium dependence of the velocity, V, at which TFs are propelled over a bed of skeletal myosin in the presence of myosin ATPase inhibitors (to vary r) and at different myosin surface densities (to vary N). We show that the experimentally observed Nr dependencies of pCa_{50} and n_H are consistent with model predictions.

In striated muscle, the pCa_{50} must be comparable to the calcium concentration in the myocyte cytoplasm during contraction, and maximizing TF cooperativity minimizes the amount of calcium that needs to be pumped out of the cytoplasm during relaxation. However, little is known about the factors that optimize pCa_{50} and n_H in striated muscle. Our results indicate that pCa_{50} varies linearly with Nr and that n_H reaches a maximal value at a duty ratio consistent with that measured for skeletal and cardiac myosin. These results suggest that disease states that alter actin−myosin ATPase kinetics may

dx.doi.org/10.1021/bi400262h | *Biochemistry* 2013, 52, 6437−6444

indirectly affect calcium responsiveness and thus the energetics of calcium regulation in muscle cells. Proteins and protein modifications that influence actin−myosin ATPase kinetics may provide compensatory mechanisms.

MATERIALS AND METHODS

Protein Preparations. Skeletal muscle myosin was prepared from rabbit psoas as previously described and stored in glycerol at −20 °C.[26,27] Actin was purified from rabbit psoas and stored on ice at 4 °C.[28] For *in vitro* motility assays, 1 μM actin was incubated with 1 μM tetramethyl-rhodamine isothiocyanate (TRITC) phalloidin overnight at 4 °C. Troponin and tropomyosin (TmTn) were purified from rabbit skeletal muscle as previously described.[29,30] Actin (1 μM) was incubated with 100 nM TmTn for 10−15 min prior to use.

Buffers. Myosin buffer contained 300 mM KCl, 25 mM imidazole, 1 mM EGTA, 4 mM $MgCl_2$, and 10 mM DTT. Actin buffer contained 50 mM KCl, 50 mM imidazole, 2 mM EGTA, 8 mM $MgCl_2$, and 10 mM DTT. For all motility experiments, motility buffer (25 nM TmTn, 50 mM KCl, 50 mM imidazole, 2 mM EGTA, 8 mM $MgCl_2$, 10 mM DTT, and 0.5% methylcellulose) was used at 1 mM ATP. An 80% (w/v, 2.34 M) sucrose stock solution was made by slowly dissolving sucrose [>99.5% pure (Sigma-Aldrich, St. Louis, MO)] in distilled water. Amrinone (Sigma-Aldrich) was prepared in 0.5 M lactic acid at a concentration of 214 mM, as previously described.[31] Motility buffers were brought to pH 7.4 using NaOH. All solutions except myosin buffer contained an oxygen scavenger (~6 mg/mL glucose, 0.03 mg/mL glucose oxidase, or 0.05 mg/mL catalase) that was added immediately prior to imaging to minimize pH changes due to the oxidation of glucose to gluconic acid.[32]

***In Vitro* Motility Assay.** The sliding velocity of fluorescently labeled thin filaments over a bed of myosin molecules was measured at 30 °C, as previously described.[16] Myosin (25 and 100 μg/mL) in myosin buffer was adhered to a nitrocellulose-coated glass surface. Nonspecific binding of protein to the surface was inhibited with bovine serum albumin (0.5 mg/mL). Labeled actin (as reconstituted thin filaments) (approximately 10 nM) was next added, followed by motility buffer. The pCa of the motility buffer was varied as a function of free calcium using Bathe Software to calculate calcium concentrations. To vary myosin density, the concentration of myosin in the myosin buffer was varied as previously described.[16] It is estimated that there are 2092 heads/μm^2 at 100 μg/mL, where at 25 μg/mL there are approximately 700 heads/μm^2.[20]

Motility assays were performed using a Nikon TE2000 epifluorescence microscope with fluorescence images digitally acquired with a Roper Cascade 512B camera (Princeton Instruments, Trenton, NJ). For each flow cell, we recorded three 30 s image sequences from three different fields, each containing 20−40 actin filaments. Data obtained from these three fields constituted one (n = 1) experiment.

Image Tracking. The image capture rate was adjusted for the observed velocity. Fast phase velocities ($V > V_{pCa_{50}}$) were captured at 10 fps (frames per second). Slow phase velocities were captured between 5 and 10 fps, depending on the condition. For each image sequence, objects were segmented from the background using binary threshold and their positions were calculated using SimplePCI Software for Image Acquisition and Analysis (Hamamatsu Corp., Sewickley, PA) IPA-MTA (Motion Tracking and Analysis) centroid algorithm. Intersecting trajectories were excluded from the analysis. Noisy filament movements (i.e., filament reptation) were mitigated and excluded where possible via a minimal displacement threshold of 5 μm over a 30 s window. The lower-resolution limit of ≈0.15 μm/s and ≈3% motile filaments were determined from zero calcium (i.e., nonmotile) conditions and used to filter smoothly moving filaments (Table 1).

Table 1[a]

	% motile at pCa 4 (±SD)	% motile at pCa 7 (±SD)	pCa_{50} (±SE)	n_H (±SE)
control	62.7 ± 4.6	2.4 ± 1.5	6.03 ± 0.04	2.7 ± 0.4
60 mM sucrose	38.6 ± 8.0	2.3 ± 0.6	6.1 ± 0.1	2.0 ± 0.9
120 mM sucrose	58.6 ± 6.5	0.6 ± 0.3	5.85 ± 0.03	1.3 ± 0.4
2 mM amrinone	39.4 ± 7.9	6.5 ± 2.8	6.06 ± 0.09	2.3 ± 0.9
4 mM amrinone	45.5 ± 7.9	19.9 ± 10.3	6.5 ± 0.1	1.3 ± 0.4
4 mM amrinone and 120 mM sucrose	49.6 ± 0.7	4.19 ± 0.08	5.9 ± 0.06	3.0 ± 0.8
4m amrinone and reduced myoinositol	43.5 ± 3.7	0.29 ± 0.14	5.9 ± 0.1	3.5 ± 1.4

[a]The fraction of smoothly motile filaments was determined using a minimal displacement threshold and the lower limit of resolution from image analysis (see Materials and Methods). Expectedly, addition of amrinone increases the fraction of moving filaments at low calcium concentrations (pCa 7), while addition of sucrose reduced the fraction of motile filaments. Calcium sensitivity and cooperativity values are enhanced when compared to V−pCa analysis, which is commonly observed with this analysis;[24] however, the trends in pCa_{50} and n_H changes are consistent with V−pCa analysis (Figure 6 and Table 2).

Simulations. A Markov chain Monte Carlo simulation was implemented in C++; the code was compiled with the GNU C ++ compiler, and the simulations to reduce computation time were run on a cluster composed of Sun Fire X4100, X4140, X4200, and X4600 servers as compute nodes. The simulation was based on a two-state model (Figure 2A) similar to that proposed by Huxley.[33] Transition probabilities for attachment of myosin to and detachment of myosin from the TF were determined from attachment, Nk_{att}' (eq 1), and detachment, k_{det}, kinetic rates, where N is the number of myosin heads available to bind a TF regulatory unit. V was calculated for all time steps at which the number of myosin heads strongly bound to the TF, N_b, is greater than zero. Each simulated velocity was obtained from an average of ten 50 s simulations. The simulation is spatially inexplicit and assumes only one regulatory unit. The regulatory unit is the minimal length of the TF modeled by the parameters in eq 1. The simulated calcium dependence of V was analyzed using a Levenberg−Marquardt minimization algorithm for the Hill function $[V = V_{min} + ((V_{max} - V_{min})/\{1 + 10^{[\log(pCa_{50}-pCa)]^{nH}}\})]$.

Fitting Experimental Data. We used our model to determine kinetic parameters for experimental V−pCa data sets as follows. The calcium dependence of V was simulated over a wide range of k_{att}, k_{det}, and N values and analyzed to obtain values for pCa_{50}, n_H, and V_{max} as described above. Experimental V−pCa relationships were also fit to the Hill

dx.doi.org/10.1021/bi400262h | *Biochemistry* 2013, 52, 6437−6444

Table 2[a]

	no. of simulations	experimental control	60 mM sucrose	120 mM sucrose	2 mM amrinone	4 mM amrinone	120 mM sucrose and 4 mM amrinone	N reduction with 4 mM amrinone
N	10, 30, 50	30	30	30	30	30	30	2
k_{att} (s^{-1} $head^{-1}$)	0−60	30	19	12	30	30	13	30
k_{basal} (s^{-1} $head^{-1}$)	0.001	0.001	0.001	0.001	0.001	0.001	0.001	0.001
k_{det} (s^{-1})	0−1000	375	375	375	300	235	235	200
$N_{1/2}$	2	2	2	2	2	2	2	2
K_{Ca} (μM)	5.5	2	2.5	4.5	1.65	0.7	2.2	2
p	2	1.8	1.1	0.85	1.8	1.15	2.35	2.75
f_c	0.85	0.85	0.85	0.85	0.85	0.85	0.85	0.85
f_m	0.65	0.65	0.65	0.65	0.65	0.65	0.65	0.65
V_{max} (μm/s)		3.36	2.80	2.16	2.26	2.31	1.83	0.43
pCa_{50}		5.77	5.59	5.22	5.90	6.40	5.66	5.62
n_H		2.39	1.45	1.07	2.37	1.60	3.13	3.42

[a]Parameters obtained from model simulations (above empty row) and from Hill fits to experimental data (below empty row). All model parameters with the exception of $N_{1/2}$, f_c, and f_m are within the range of reported values.[17] N is the number of heads accessible to bind a regulatory unit during stochastic simulation, and the control value of 30 myosin heads is consistent with previous studies. Myosin attachment (k_{att}) and detachment (k_{det}) rate constants for the control are consistent with reported values. The TnC−Ca^{2+} affinity, K_{Ca}, and the cooperative coefficient, p, are consistent with reported values and were allowed to vary only when changes in TF−myosin ATPase kinetics were not sufficient to account for observed changes in pCa_{50} or n_H.[22,23]

function (above) to obtain experimental pCa_{50}, n_H, and V_{max} values. These experimental parameters were compared with simulated parameters to obtain a best fit. First, all simulated data sets having pCa_{50} values that were the same as the experimental pCa_{50} values were selected. Next, from this subset, all simulated data sets with n_H values that were the same as the experimental n_H values were selected. Finally, from this subset, all simulated data sets having V_{max} values that were the same as the experimental V_{max} values were selected. This typically resulted in a set of V−pCa curves that were simulated with similar k_{att}, k_{det}, and N values. Each of these parameters was averaged over all selected data sets to obtain the modeled k_{att}, k_{det}, and N values for a given V−pCa experiment.

RESULTS

We developed a Markov chain, Monte Carlo simulation based on the two-state model in Figure 2A. The effective rate of TF−myosin binding (k_{att}') for the simulation is defined as a fraction of a maximal rate of attachment (k_{att}) by eq 1:

$$k_{att}' = k_{att}\left(f_c \frac{[Ca^{2+}]^p}{[Ca^{2+}]^p + K_{Ca}{}^p} + f_m \frac{N_b}{N_b + N_{1/2}}\right) + k_{basal} \quad (1)$$

At a low calcium concentration and with no myosin heads strongly bound to the TF ($N_b = 0$), we assume a basal rate of myosin attachment, k_{basal}. The calcium sensitivity of k_{att}' is calculated as a Hill function (Figure 2B), where p is the cooperative coefficient for calcium binding and K_{Ca} is the K_d for TnC−calcium binding. Although K_{Ca} and p have both been shown to change with the addition of myosin,[22−24] for the sake of simplicity here we assume that K_{Ca} and p are independent of myosin activation (Table 2). These constants are allowed to vary only when ATPase kinetics are insufficient to account for observed changes in pCa_{50} or n_H.

The N_b dependence of k_{att}' is defined as a hyperbolic function (Figure 2C), where $N_{1/2}$ is the number of TF-bound myosin heads required for half-maximal myosin activation of the TF. The fractional contributions (i.e., relative effect) of calcium- and myosin-dependent activation, f_c and f_m, respectively, describe the extent to which calcium or myosin binding alone can activate the thin filament. There appears to be a disparity between the relative importance of calcium and strong binding activation for skeletal and cardiac myosin. Cardiac myosin appears to be more affected by crossbridge activation.[34,35] The values of f_c and f_m can be adjusted to account for such differences, and the sum of these coefficients for fractional activation need not equal 1. Here we assume that the calcium and myosin dependencies of k_{att}' are independent (eq 1) to simplify the model and to demonstrate that observed changes in TF cooperativity, n_H, can result from changes in either myosin-based or calcium-based activation. This model can easily be modified to include an interdependence of the calcium- and myosin-based terms (e.g., a myosin-induced change in calcium−TnC affinity).

The simulation limits k_{att}' to a maximal value of k_{att}. Fractional activation, A_f, is then defined by eq 2:

$$A_f = \frac{k_{att}'}{k_{att}} \leq 1 \quad (2)$$

Simulated TF sliding velocities are calculated from eq 3:

$$V = dk_{det}A_f \quad (3)$$

so that

$$V = dk_{det}\frac{k_{att}'}{k_{att}} = dk_{det}\left(f_c \frac{[Ca^{2+}]^p}{[Ca^{2+}]^p + K_{Ca}{}^p} + f_m \frac{N_b}{N_b + N_{1/2}} + \frac{k_{basal}}{k_{att}}\right) \quad (4)$$

We assume the maximal TF sliding velocity, V_{max}, is the product of the average myosin step size (d) and the rate of TF−myosin detachment (k_{det}). The partially activated velocity, V, is calculated as the product of V_{max} and A_f. To determine pCa_{50} and n_H, simulations were fit to the Hill function. To estimate

dx.doi.org/10.1021/bi400262h | Biochemistry 2013, 52, 6437−6444

model parameters from experimental data, simulations that best represented the data were chosen from a library (Table 2).

We used this simple, cooperative model of TF regulation to simulate the pCa dependence of TF sliding velocity (V–pCa curves) for a wide range of k_{att}, k_{det}, and N values (Table 2, simulations). Each simulated V–pCa curve was fit to the Hill equation (see Materials and Methods) to determine values for pCa_{50} and n_H. These values were then plotted as a function of r (Figures 3 and 4) at three different values of N.

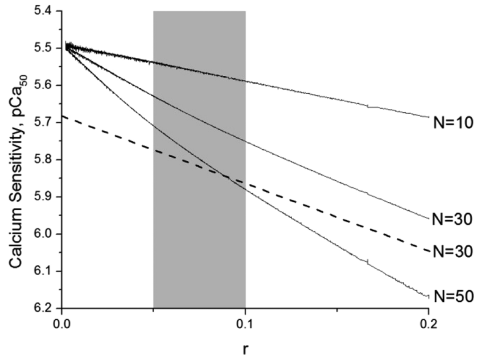

Figure 3. Effects of duty ratio on TF calcium sensitivity. Simulations of V–pCa curves were obtained (Table 2) for many permutations of ATPase kinetic parameters (k_{att} = 0–60 s^{-1} $head^{-1}$, and k_{det} = 0–1000 s^{-1}), and pCa_{50} values were obtained from Hill fits to each curve. When plotted against duty ratio (r), pCa_{50} varies linearly with a slope that is proportional to N (the number of myosin heads available for binding). The pCa_{50}–r dependence of k_{att}' (---) shows a y-intercept at pK_{Ca} (Table 2). The disparity between the points of the intercept (5.5 vs 5.7) arises in the calculation of detachment-limited velocity (eq 3). The shaded area represents the estimated range of physiological duty ratios (5–10%) for striated muscle myosin.[20]

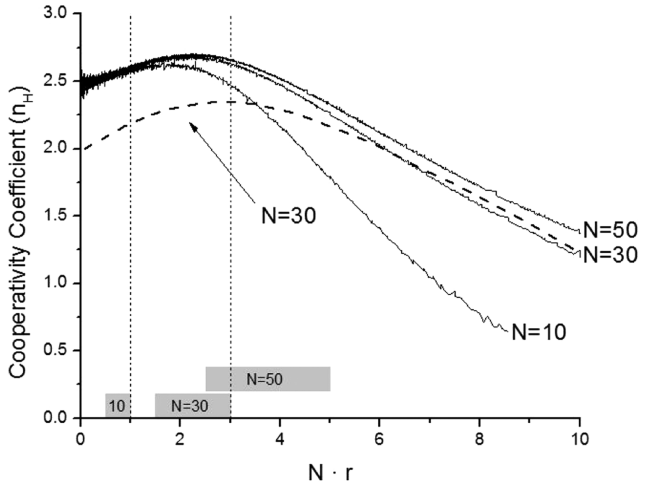

Figure 4. Effects of duty ratio on TF cooperativity. Simulations of V–pCa curves were obtained (Table 2) for many permutations of ATPase kinetic parameters (k_{att} = 0–60 s^{-1} $head^{-1}$, and k_{det} = 0–1000 s^{-1}), and n_H values were obtained from Hill fits to each simulated curve. The cooperative coefficient initially increases with increasing Nr (—), reaching a maximum within the estimated range (0.05–0.10) of physiological duty ratios (shaded boxes). A maximal n_H is achieved within the range of 1–3 myosin heads strongly bound to the TF at maximal activation (---). The n_H–Nr dependence of k_{att}' (---) shows a y-intercept equivalent to p in the simulation (Table 2), which differs from the n_H–Nr dependence of V (black lines) due to the calculation of detachment-limited velocity (eq 3).

Figure 3 shows that at a fixed number of myosin heads, N, available to bind a TF regulatory unit, pCa_{50} varies linearly with myosin duty ratio:

$$pCa_{50} \cong pCa_{50}' + \beta(Nr) \quad (5)$$

where β is a proportionality constant that depends on model parameters f_m, f_c, and $N_{1/2}$ and pCa_{50}' is the y-intercept for this linear relationship. The myosin duty ratio, r, is defined in eq 6.

$$r = \frac{k_{att}}{k_{att} + k_{det}} \quad (6)$$

The two principal terms in eq 5 reflect the calcium- and myosin-dependent terms in eq 1. In the range of physiological duty ratios reported for striated muscle myosin (0.05–0.10),[20] pCa_{50} varies linearly with duty ratio, with a slope that is proportional to N (Figure 3), which is accurately described by eq 5.

Values for n_H obtained from simulations are plotted against Nr (Figure 4), showing that TF cooperativity, like pCa_{50}, varies with myosin duty ratio, reaching a maximal value within a physiological range of r (Figure 4, bars). n_H values are significantly reduced at high duty ratios and high N values.

To test model efficacy (eq 4) and eq 5, we used IVM to determine the effects of substrate and small molecule inhibition of myosin ATPase on V–pCa curves. Equation 5 can be rewritten to express a change in pCa_{50}, ΔpCa_{50}, relative to a control value following a chemical perturbation as

$$\Delta pCa_{50} = \beta[(Nr)_{control} - (Nr)_{final}] = Af_{Nr} \quad (7)$$

where $A = \beta(Nr)_{control}$ and f_{Nr} is the corresponding fractional change in Nr, $[(Nr)_{control} - (Nr)_{final}]/(Nr)_{control}$, following the chemical perturbation. To test eq 7, in Figure 6A, we plot ΔpCa_{50} versus f_{Nr} for a wide range of perturbations.

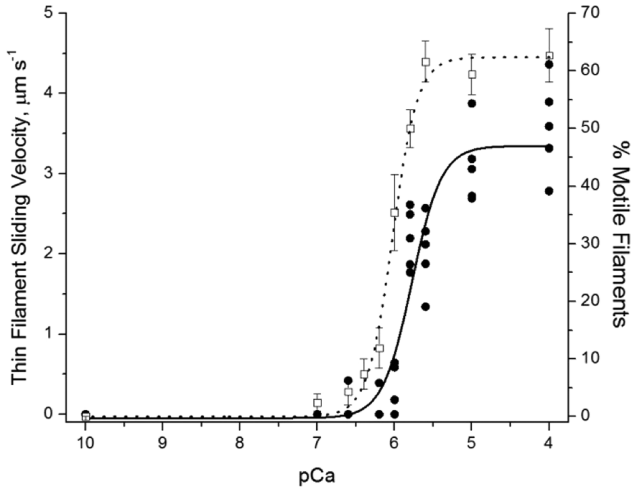

Figure 5. Calcium sensitivity and cooperativity of TF activation measured using IVM. TF velocities under control conditions were measured at different calcium concentrations and plotted as a function of pCa. V–pCa curves were fit to the Hill equation (●, solid line) to obtain values for pCa_{50} (5.77 ± 0.046) and n_H (2.28 ± 0.549). To obtain model kinetic parameters (Table 2), we chose simulated V–pCa curves from a library that most accurately described the Hill fit. Each data point represents an independent experiment. The percent of motile filaments (□, dashed line) was determined from a minimal displacement threshold and the lower limit of image resolution (see Materials and Methods).

dx.doi.org/10.1021/bi400262h | Biochemistry 2013, 52, 6437–6444

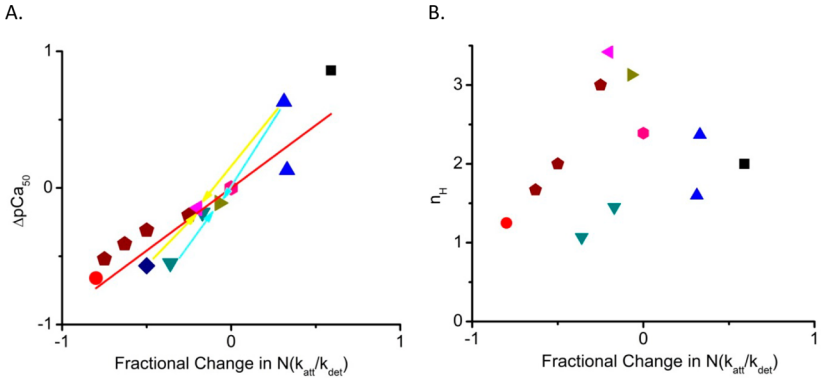

Figure 6. Effects of k_{att}, k_{det}, and N on pCa_{50} and n_H. (A) Changes in pCa_{50}, ΔpCa_{50}, observed upon addition of kinetic effectors are plotted vs the corresponding fractional change in the kinetic parameter Nr. These effectors include subsaturating 50 μM ATP (black square), addition of 2 and 4 mM amrinone (blue triangles), addition of 1.6 μM blebbistatin (red circle), the different myosin densities reported by Gorga et al.[16] (pentagons), a 25 μg/mL myosin incubation (blue diamond), 60 and 120 mM sucrose (upside-down triangles), combined addition of 4 mM amrinone and 120 mM sucrose (right-pointing triangle), and combined addition of 4 mM amrinone and 25 μg/mL myosin incubation (left-pointing triangle). The control experiment (hexagon) is plotted as (0,0). The yellow arrows point from the individual ΔpCa_{50} values obtained for 4 mM amrinone and 120 mM sucrose to the ΔpCa_{50} obtained from the combination of these inhibitors, illustrating the compensatory effects predicted by eq 7. The cyan arrows point from the individual ΔpCa_{50} for 4 mM amrinone and 25 μg/mL myosin to the ΔpCa_{50} obtained from the combination of these inhibitors, illustrating the compensatory effect predicted by eq 7. A linear regression that was forced through (0,0) gave a slope of 0.9 (red line). (B) Values of n_H obtained from the same experiments described in panel A plotted vs f_{Nr}. These data resemble the peak function predicted in Figure 4. We currently are unable to perform least-squares fits with our model, so statistics for describing the goodness of fit are unavailable. A comparison of pCa_{50} and n_H values obtained from both Hill fits to the data (asterisk, with SD) shows that the simulations accurately describe our experimental data.

Using IVM, we previously determined the effects of 1.6 μM blebbistatin (an inhibitor of k_{att}) and subsaturating 50 μM ATP (substrate inhibition of k_{det}) on pCa_{50} and n_H.[17] In Figure 6A, we plot the pCa_{50} shifts, ΔpCa_{50}, observed with these perturbations, estimating the corresponding f_{Nr} values from either kinetic studies (1.56 μM blebbistatin results in an ~80% decrease in k_{att}) or changes in V (decreasing the ATP concentration to 50 μM results in an ~60% decrease in V and thus k_{det}).

To further test eq 7, here we also measure the effects of the inhibitor, amrinone, on pCa_{50} and n_H (Supporting Information, Figures 1 and 2). Amrinone slows k_{det} either by slowing the rate of ADP release or by increasing the rate of binding of ADP to actin-bound myosin.[31,36] In Figure 6A, we plot pCa_{50} shifts, ΔpCa_{50}, observed upon addition of both 2 and 4 mM amrinone and estimate the corresponding changes in f_{Nr} from our observed changes in V (2 and 4 mM amrinone slow V and thus k_{det} by 33 and 31%, respectively). By increasing the affinity of ADP for myosin, amrinone slows k_{det} by increasing the amount of time myosin spends in the AMD state rather than the time it spends in the rigor state. Our results (Figure 6A) show that decreasing k_{det} has a similar effect on pCa_{50} regardless of whether k_{det} was slowed by increasing the time spent in AM or whether it was slowed by increasing the time spent in AMD. To further test eq 7, here we measured the effects of sucrose, a kinetic inhibitor of k_{att}, on V, pCa_{50}, and n_H. We have shown, in a manuscript submitted for publication, that sucrose specifically inhibits the rate of AM strong bond formation (k_{att}). Specifically, using stopped-flow fluorimetry, we have shown that 880 mM sucrose slows k_{att} 5-fold without significantly inhibiting any other step in the ATPase reaction cycle. Most importantly, 880 mM sucrose has no significant effect on k_{det}. In Figure 6A, we plot pCa_{50} shifts, ΔpCa_{50}, observed upon addition of both 60 and 120 mM sucrose (Supporting Information, Figures 3 and 4) and estimate the corresponding changes in f_{Nr} from changes in V (60 and 120 mM sucrose slow V by 17 and 36%, respectively). Figure 6A shows that decreasing k_{att} has a similar effect on pCa_{50} regardless of whether k_{att} was slowed by blebbistatin or sucrose.

Equation 7 predicts that ΔpCa_{50} varies proportionally with fractional changes in N. This relationship can be tested by decreasing the myosin surface density in the IVM assay, which can be achieved by decreasing the incubation concentration of myosin. In Figure 6A, we plot ΔpCa_{50} values that we obtained at low myosin densities as well as values estimated from pCa−V curves reported by Gorga et al.[16] In both cases, we calculated f_{Nr} as the fractional change in the incubation concentration, which according to Harris and Warshaw[20] is similar to the fractional change in surface density and thus in N. Interestingly, we observe that changes in pCa_{50} saturate at incubation concentrations greater than 50 μg/mL, so we calculate f_{Nr} relative to the pCa_{50} obtained at 50 μg/mL.

Equation 7 predicts that a ΔpCa_{50} resulting from a fractional change in a given kinetic parameter (k_{att}, k_{det}, or N) can be reversed by a similar fractional change in another kinetic parameter. Consistent with this prediction, we showed that the pCa_{50} shift induced upon addition of 4 mM amrinone is reversed upon further addition of 120 mM sucrose (Supporting Information, Figure 5 and Figure 6A, cyan arrows). The assumption that we make in estimating f_{Nr} for this experiment is that the effect of sucrose on k_{att} is unaffected by amrinone, and similarly, the effect of amrinone on k_{det} is unaffected by sucrose. Similarly, we showed that the pCa_{50} shift induced via the addition of 2 mM amrinone is also reversed by decreasing myosin density (i.e., N) by decreasing the incubation concentration from 50 to 25 μg/mL (Supporting Information, Figure 6 and Figure 6A, yellow arrows). According to Harris and Warshaw,[20] this results in an ~50% decrease in N.

Taken together, the data in Figure 6A show a linear relationship between ΔpCa_{50} and f_{Nr}, consistent with eqs 5 and 7. A linear fit to these data (Figure 6B, red line) gives a slope of A = 0.9 (eq 7).

dx.doi.org/10.1021/bi400262h | *Biochemistry* 2013, 52, 6437−6444

The n_H values obtained from the experiments described above are plotted versus f_{Nr} in Figure 6B and appear to exhibit the peak relationship predicted in Figure 4.

Our model indicates that both pCa_{50} and n_H can be altered predictably by changing actin−myosin ATPase kinetics in the absence of an effect on TnC−calcium binding cooperativity or affinity. Our data support the idea that disease states that alter actin−myosin ATPase kinetics will affect calcium sensitivity in striated muscle predictably.[37] Similarly, calcium sensitivity can be modulated through inhibitors, activators, protein modifications (e.g., myosin phosphorylation), and accessory sarcomeric proteins (e.g., MyBP-C) that affect actin−myosin ATPase kinetics.

DISCUSSION

We have developed and experimentally tested a simple model of striated muscle regulation that accurately describes the calcium- and myosin-dependent activation of TFs. The model is based on a two-state kinetic scheme (Figure 2A) that resembles Huxley's model[33] and describes TF regulation using a chemical kinetic formalism that incorporates mesoscopic parameters appropriate for modeling macroscopic muscle mechanics rather than unconstrained structural parameters. Our model predicts that pCa_{50} varies linearly as Nr (Figure 3) and that n_H varies with Nr as a peak function, reaching a maximal value near the range of duty ratios reported for cardiac and skeletal myosin (Figure 4).

Equation 5 predicts that any modification that increases the number of myosin heads, Nr, strongly bound to a regulatory unit of a TF during maximally activated ATPase results in a proportional increase in pCa_{50}. The duty ratio, r, is a function of both k_{att} and k_{det} (eq 6), and previous studies are consistent with the predicted k_{det} dependence of pCa_{50}, showing that extending the lifetime of strongly bound crossbridges (i.e., decreasing k_{det}) increases pCa_{50}.[3,12,13,15−17] Our model predicts that the k_{det} dependence of pCa_{50} is not unique to rigor activation, and this is supported by our observation that, like the effects of rigor heads and NEM-S1, amrinone (an inhibitor of ADP release) activates the TF in the absence of calcium.

The effects of k_{att} on pCa_{50} predicted by eq 5 are less well studied. Our first indication that both k_{att} and k_{det} influenced pCa_{50} came from our observation that the pCa_{50} for TF sliding velocities was similar for skeletal and smooth muscle myosin-based motility (data not shown). These findings suggested that, consistent with eq 5, the effect of smooth muscle myosin's slower k_{det} on pCa_{50} is offset by a slower k_{att} (smooth and skeletal muscle myosin exhibit similar duty ratios).[20] In Figure 6, we showed that, consistent with eq 5, pCa_{50} shifts with a change in any one of the kinetic parameters (N, k_{det}, or k_{att}), and this shift can be reversed with a change in any other of these parameters. The maximal pCa_{50} is limited by a maximal duty ratio, r, of 1 and a saturating number, N, of actin-bound myosin heads. The lower limit for pCa_{50} is the myosin-independent calcium sensitivity, pK_{Ca}.

Observed changes in n_H for TF activation are often interpreted as changes in the cooperative binding of calcium to TnC; however, our simulations and data suggest that n_H is also influenced by TF−myosin ATPase kinetics (Figures 4 and 6). The predicted increase in n_H with an increasing Nr (Figure 4) results from myosin activation of the TF, whereas the predicted decrease in n_H at high values of Nr is caused by the slope of calcium-dependent activation becoming shallow at high levels of myosin activation (Figure 2B). The existence of an optimal n_H (Figures 4 and 6) is physiologically significant. Specifically, any protein mutation or modification that decreases n_H by altering ATPase kinetics will increase the amount of calcium that must be removed from the cytoplasm to relax muscle, resulting in potential metabolic challenges.

Our experimental data, showing the effects of k_{att}, k_{det}, and N on pCa_{50} and n_H (Figure 6), are consistent with our model predictions (Figures 3 and 4) with one exception. The decrease in n_H observed upon addition of sucrose (Figure 6B) is significantly greater than that predicted by our model (Figure 4). Our simulations account for this discrepancy via a k_{att} dependence of both p and K_{Ca}, suggesting that in addition to its effects on both n_H and pCa_{50} through altered ATPase kinetics (Figures 3 and 4), k_{att} affects n_H and pCa_{50} through a k_{att}-dependent calcium−TnC dissociation constant (K_{Ca}) and cooperative coefficient (p) as previously reported.[22,23]

Models of myocyte contractility often treat myofibrils as a black box that responds to calcium in a simple, well-defined way that is independent of actin−myosin ATPase activity. The observation that TF−myosin ATPase kinetics influences both calcium sensitivity and cooperativity implies that an explicit description of ATPase kinetics is required of any accurate model of myocyte contractility. In short, treating muscle myofibrils as passive, calcium-sensitivive elements is an inaccurate oversimplification. The model presented here provides an easily implemented alternative approach for explicitly describing how pCa_{50} and n_H are tuned by actin−myosin ATPase kinetics.

ASSOCIATED CONTENT

Supporting Information

The supporting information contains pCa-velocity and pCa-motile-filament data (symbols) obtained from in vitro motility experiments as well as fits of these data to our model (solid line). Values for pCa_{50} and n obtained from these fits are summarized in the main body of the manuscript. This material is free of charge via the Internet at http://pubs.acs.org.

AUTHOR INFORMATION

Corresponding Author

*Department of Biochemistry and Molecular Biology, University of Nevada School of Medicine, 1664 N. Virginia St., MS 330/HMS 163, Reno, NV 89557. E-mail: jebaker@unr.edu. Telephone: (775) 784-4103.

Funding

This work was supported in part by National Institutes of Health Grants 1R01HL090938-01A1 (to J.E.B.) and 1R01AR061149 (to C.R.C. and J.E.B.).

Notes

The authors declare no competing financial interest.

ACKNOWLEDGMENTS

We thank Dr. Kevin Facemyer for valuable guidance, Dr. Ellen Webb and Andrew Manfra for critical reading of the manuscript and helpful discussions, and Jasper Bedaux for porting the MT pseudorandom number generator to C++.

ABBREVIATIONS

TF, thin filament; M, myosin; N, number of myosin heads available for binding; r, duty ratio; n_H, Hill cooperativity coefficient; NEM, N-ethylmaleimide; pCa, calcium concentration as $-\log[Ca^{2+}]$; pCa_{50}, measure of calcium sensitivity;

Tm, tropomyosin; TnC, troponin C; k_{att}, rate of myosin attachment; k_{det}, rate of myosin detachment; SD, standard deviation; SE, standard error.

REFERENCES

(1) Hill, T., and Eisenberg, E. (1980) Theoretical considerations in the equilibrium binding of myosin fragments on F-actin. *Biophys. Chem.*, 271−281.

(2) Lehrer, S. (1994) The regulatory switch of the muscle thin filament: Ca^{2+} or myosin heads? *J. Muscle Res. Cell Motil. 15*, 232−236.

(3) Swartz, D. R., Moss, R. L., and Greaser, M. L. (1996) Calcium alone does not fully activate the thin filament for S1 binding to rigor myofibrils. *Biophys. J. 71*, 1891−1904.

(4) Huxley, H. (1973) Structural Changes in the Actin-and Myosin-containing Filaments during Contraction. *Cold Spring Harbor Symp. Quant. Biol. 37*, 361−376.

(5) Haselgrove, J. (1975) X-ray evidence for a conformational change in the actin-containing filaments of vertebrate striated muscle. *J. Mol. Biol.*, 113−143.

(6) Parry, D. A., and Squire, J. M. (1973) Structural role of tropomyosin in muscle regulation: Analysis of the X-ray diffraction patterns from relaxed and contracting muscles. *J. Mol. Biol. 75*, 33−55.

(7) Squire, J. (1994) The actomyosin interaction-shedding light structural events: "Plus ca change, plus c"est la meme chose'. *J. Muscle Res. Cell Motil. 231*, 227−231.

(8) Phillips, G., Fillers, J., and Cohen, C. (1986) Tropomyosin crystal structure and muscle regulation. *J. Mol. Biol. 192*, 111−131.

(9) Houdusse, A., Love, M. L., Dominguez, R., Grabarek, Z., and Cohen, C. (1997) Structures of four Ca^{2+}-bound troponin C at 2.0 Å resolution: Further insights into the Ca^{2+}-switch in the calmodulin superfamily. *Structure 5*, 1695−1711.

(10) McKillop, D., and Geeves, M. (1993) Regulation of the interaction between actin and myosin subfragment 1: Evidence for three states of the thin filament. *Biophys. J. 65*, 693−701.

(11) Smith, D., and Geeves, M. (2003) Cooperative regulation of myosin-actin interactions by a continuous flexible chain II: Actin-tropomyosin-troponin and regulation by calcium. *Biophys. J. 84*, 3168−3180.

(12) Bremel, R., and Weber, A. (1972) Cooperation within actin filament in vertebrate skeletal muscle. *Nature 238*, 97−101.

(13) Swartz, D., and Moss, R. (1992) Influence of a strong-binding myosin analogue on calcium-sensitive mechanical properties of skinned skeletal muscle fibers. *J. Biol. Chem. 267*, 20497−20506.

(14) Fitzsimons, D. P., and Moss, R. L. (1998) Strong Binding of Myosin Modulates Length-Dependent Ca^{2+} Activation of Rat Ventricular Myocytes. *Circ. Res.*, 602−607.

(15) Kad, N., Kim, S., Warshaw, D., VanBuren, P., and Baker, J. (2005) Single-myosin crossbridge interactions with actin filaments regulated by troponin-tropomyosin. *Proc. Natl. Acad. Sci. U.S.A. 102*, 16990−16995.

(16) Gorga, J., Fishbaugher, D., and VanBuren, P. (2003) Activation of the calcium-regulated thin filament by myosin strong binding. *Biophys. J. 85*, 2484−2491.

(17) Sich, N. M., O'Donnell, T. J., Coulter, S. A., John, O. A., Carter, M. S., Cremo, C. R., and Baker, J. E. (2011) Effects of Actin-Myosin Kinetics on the Calcium Sensitivity of Regulated Thin Filaments. *J. Biol. Chem. 285*, 39150−39159.

(18) Geeves, M., Griffiths, H., Mijailovich, S., and Smith, D. (2011) Cooperative $[Ca^{2+}]$-dependent regulation of the rate of myosin binding to actin: Solution data and the tropomyosin chain model. *Biophys. J. 100*, 2679−2687.

(19) Trybus, K. M., and Taylor, E. W. (1980) Kinetic studies of the cooperative binding of subfragment 1 to regulated actin. *Proc. Natl. Acad. Sci. U.S.A. 77*, 7209−7213.

(20) Harris, D., and Warshaw, D. (1993) Smooth and skeletal muscle myosin both exhibit low duty cycles at zero load in vitro. *J. Biol. Chem. 268*, 14764−14768.

(21) Bremel, R., and Weber, A. (1975) Calcium binding to rabbit skeletal myosin under physiological conditions. *Biochim. Biophys. Acta 376*, 366−374.

(22) Grabarek, Z., Grabarek, J., Leavis, P. C., and Gergely, J. (1983) Cooperative binding to the Ca^{2+}-specific sites of troponin C in regulated actin and actomyosin. *J. Biol. Chem. 258*, 14098−14102.

(23) Grabarek, Z., Tao, T., and Gergely, J. (1992) Molecular mechanism of troponin-C function. *J. Muscle Res. Cell Motil. 13*, 383−393.

(24) Gordon, A., Homsher, E., and Regnier, M. (2000) Regulation of contraction in striated muscle. *Physiol. Rev. 80*, 853−924.

(25) Guth, K., and Potter, J. (1987) Effect of rigor and cycling cross-bridges on the structure of troponin C and on the Ca^{2+} affinity of the Ca^{2+}-specific regulatory sites in skinned rabbit psoas fibers. *J. Biol. Chem. 262*, 13627−13635.

(26) Prochniewicz, E., Lowe, D., Spakowicz, D. J., Higgins, L., O'Conor, K., Thompson, L. V., Ferrington, D. A., and Thomas, D. D. (2008) Functional, structural, and chemical changes in myosin associated with hydrogen peroxide treatment of skeletal muscle fibers. *Am. J. Physiol. 294*, C613−C626.

(27) Margossian, S. S., and Lowey, S. (1982) Preparation of myosin and its subfragments from rabbit skeletal muscle. In *Methods in Enzymology* (Colowick, S. P., and Kaplan, N. O., Eds.) pp 55−71. Academic Press, New York.

(28) Pardee, J., and Spudich, J. (1982) Purification of muscle actin. *Methods Enzymol. 85*, 164−181.

(29) Potter, J. D. (1982) Preparation of troponin and its subunits. *Methods Enzymol. 85*, 241−263.

(30) Smillie, L. (1982) Preparation and Identifaction of Alpha and Beta Tropomyosins. *Methods Enzymol. 85*, 234−241.

(31) Klinth, J., Arner, A., and Månsson, A. (2003) Cardiotonic bipyridine amrinone slows myosin-induced actin filament sliding at saturating [MgATP]. *J. Muscle Res. Cell Motil. 24*, 15−32.

(32) Shi, X., Lim, J., and Ha, T. (2010) Acidification of the oxygen scavenging system in single-molecule fluorescence studies: In situ sensing with a ratiometric dual-emission probe. *Anal. Chem. 82*, 6132−6138.

(33) Huxley, A. F. (1957) Muscle Structure and Theories of Contraction. *Prog. Biophys. Biophys. Chem. 7*, 255−318.

(34) Regnier, M., Rivera, A. J., Wang, C.-K., Bates, M. A., Chase, P. B., and Gordon, A. M. (2002) Thin filament near-neighbour regulatory unit interactions affect rabbit skeletal muscle steady-state force-Ca^{2+} relations. *J. Physiol. 540*, 485−497.

(35) Gillis, T. E., Martyn, D. A., Rivera, A. J., and Regnier, M. (2007) Investigation of thin filament near-neighbour regulatory unit interactions during force development in skinned cardiac and skeletal muscle. *J. Physiol. 580*, 561−576.

(36) Albet-Torres, N., Bloemink, M., Barman, T., Candau, R., Frölander, K., Geeves, M. A., Golker, K., Herrmann, C., Lionne, C., Piperio, C., Schmitz, S., Veigel, C., and Månsson, A. (2009) Drug effect unveils inter-head cooperativity and strain-dependent ADP release in fast skeletal actomyosin. *J. Biol. Chem. 284*, 22926−22937.

(37) Moore, J. R., Leinwand, L., and Warshaw, D. M. (2012) Understanding cardiomyopathy phenotypes based on the functional impact of mutations in the myosin motor. *Circ. Res. 111*, 375−385.